Towed Streamer EM – reliable recovery of sub-surface resistivity

Allan McKay[1*], Johan Mattsson[1] and Zhijun Du[1] present a seismically guided inversion and illustrate the workflow of the data integration, which remains driven purely by the seismic and EM data.

Marine Controlled Source EM (CSEM) data has been used extensively to improve the chance of success in the search for hydrocarbons given that accumulations of oil and gas can be characterized by increased resistivity. CSEM data have been used mostly to derisk prospects. By using a Towed Streamer EM system it is possible to acquire CSEM data efficiently to determine the sub-surface resistivity at both regional and prospect scales. In addition, the simultaneous acquisition of both towed streamer seismic and EM data from the same vessel is enabled, with obvious efficiency benefits.

By performing unconstrained inversion of the Towed Streamer EM data to determine the sub-surface resistivity we aim to extract the maximum possible amount of information from the EM data before considering any constraints on the solution. In any case, in a frontier exploration setting then geological knowledge may be limited and there may be relatively few wells. In addition, we wish to ensure that the resistivity models from CSEM data can be considered an independent piece of information so that, say, any correlation between acoustic and electromagnetic structure is unforced. We present case studies that demonstrate that the subsurface resistivity determined using unconstrained inversion of Towed Streamer EM data is consistent with the logged resistivity, and the regional geological background.

Nevertheless, when assessing the prospectivity in a complex geological region, there are solution ambiguities in interpretation that cannot be addressed using a single method. The integration of seismic and CSEM data in a staged workflow, where seismic provides a high-resolution structural image of the subsurface and CSEM estimates the resistivity of assumed prospects, is potentially better able to discriminate between fluid and lithology effects than if either data set were used in isolation. The integration of seismic with CSEM can thus provide subsurface information that is either more reliable than, or simply unavailable, when only a single data type is used. In this paper we present a seismically guided inversion and illustrate the workflow of the data integration, which remains driven purely by the seismic and CSEM data. Such an integrated approach can be a powerful tool in a frontier exploration where CSEM and 3D seismic data co-exist.

It is today relatively well established that in a shallow water setting (e.g., less than about 700 m) the in-line component of the electric field induced by a Horizontal Electric Dipole (HED) source has sensitivity to both the vertical and horizontal components of resistivity (e.g., MacGregor and Tomlinson, 2014, and references therein). The case studies we outline in this paper show that we can recover both the horizontal and vertical resistivity measured in the well. Mattsson et al. (2013), demonstrated that the Towed Streamer EM sensitivity to horizontal and vertical resistivity is approximately the same, but the example was restricted to 1D – we have extended that work and show that the conclusions hold in 2D. Indeed, there is no reason to suspect that the conclusions do not extend to 3D, which is supported by case studies (e.g. Zhdanov et al., 2014) and consistent with our experience.

In addition, one of the key technical features of the Towed Streamer EM systems is dense in-line sampling of the electric field along the length of the streamer. This leads to demonstrable uplift in sensitivity to changes in sub-surface resistivity. In the final section, by comparing different in-line sampling intervals, we quantify the up-lift using illustrative examples based on a North Sea case study.

Towed Streamer EM system

The Towed Streamer EM system consists of a surface towed source and EM streamer that are towed from a single vessel. It was designed to enable efficient acquisition of CSEM data together with seismic, and can be deployed from virtually any seismic vessel.

Acquisition system

The EM source consists of an 800 m long Horizontal Electric Di-pole (HED) towed at 10 m below the sea surface beneath two surface buoys. The streamer has 72 electric field channels consisting of electrode pairs effectively providing up to 72 offsets, from 0-7700 m relative to the centre of source.

The transmitted source signal is in the form of an optimized repeated sequence (ORS) generated by an oscillating

[1] *PGS.*

[*] *Corresponding author, E-mail: Allan.McKay@pgs.com*

current of +/- 1500 Amperes. The distribution of source energy of the ORS depends on survey objectives. In general we aim for a usable frequency range of two decades spanning 0.1-10 Hz.

A source cycle lasts for 120 s. Usually the source is on for 100 s, followed by a silent period of 20 s. This 120 s cycle is what we call an EM shot. With typical acquisition speeds of between 4 and 5 knots then the in-line shot-spacing is 250-300 m.

The Towed Streamer EM system has several design features to enable maintenance of an acceptable signal-to-noise ratio. One such feature is the variation of the receiver bi-poles in length from 200 m for the nearest offset to 1100 m for the longest offset. Additional noise reduction is an important aspect; see Mattsson (2012) for more details.

The 1st generation Towed Streamer EM system is designed to work in water depths of 500 m or less, although deeper water can be considered as part of a feasibility and survey design study which is undertaken before every acquisition.

Towed Streamer EM in the Barents Sea

PGS has started to build up a substantial Towed Streamer EM multi-client library in the Barents Sea. For example, in 2014 PGS acquired nearly 12,000 km^2 of 3D Towed Streamer EM data to cover most areas of interest in the Barents Sea South East that are included in the Norwegian Sector 23rd licensing round; see Figure 1. The acquisition took less than four months. Prior to that (in 2013) nearly 850 line km of Towed Streamer EM and broadband dual sensor seismic data were acquired simultaneously using a single vessel to link together a number of known discoveries; see also McKay et al. (2014).

Unconstrained inversion workflow

Here we describe briefly some of the main features of our basic inversion workflow for 2D survey line profiles. On the ongoing inversion of the Barents Sea South East data, we are inverting each line independently using 2.5D inversion, and each area in 3D to produce a consistent set of sub-surface resistivity profiles and volumes for each area.

We use regularised unconstrained anisotropic 2.5D inversion to recover the sub-surface resistivity. The inversion code we use is the MARE2DEM code that is available via the Scripps Seafloor Electromagnetic Consortium. The forward modelling kernel of MARE2DEM is based on the adaptive finite element code of Key and Ovall (2011); the inversion scheme is based on smooth 'Occam' inversion (Constable et al., 1987), a regularized variant of Gauss-Newton minimization. In general we have found that wherever we have compared the results of unconstrained inversion of Towed Streamer EM data to the logged resistivity that anisotropic inversion is required, otherwise the resistivity sections are banded with high contrast layers and the fit of the modelled resistivity to the logged resistivity is degraded.

We typically select multiple frequency and offsets, with a first pass data selection typically covering the lowest frequencies e.g. 0.2:0.2:1 Hz, and 20 offsets in the range 1.5 to 8 km. Thereafter, we extend the frequency range to higher frequencies, aiming for a broad frequency bandwidth. The results we present in this paper are from a frequency range covering about 0.2 to 2 Hz. Wherever possible, we aim to use every source-receiver gather (with a shot-point every 250-300 m) although for long survey lines (e.g., 100-200 km) using every second source-receiver gather is usually sufficient and indeed necessary to perform the inversion in one pass while preserving a reasonable data selection and model parameterisation.

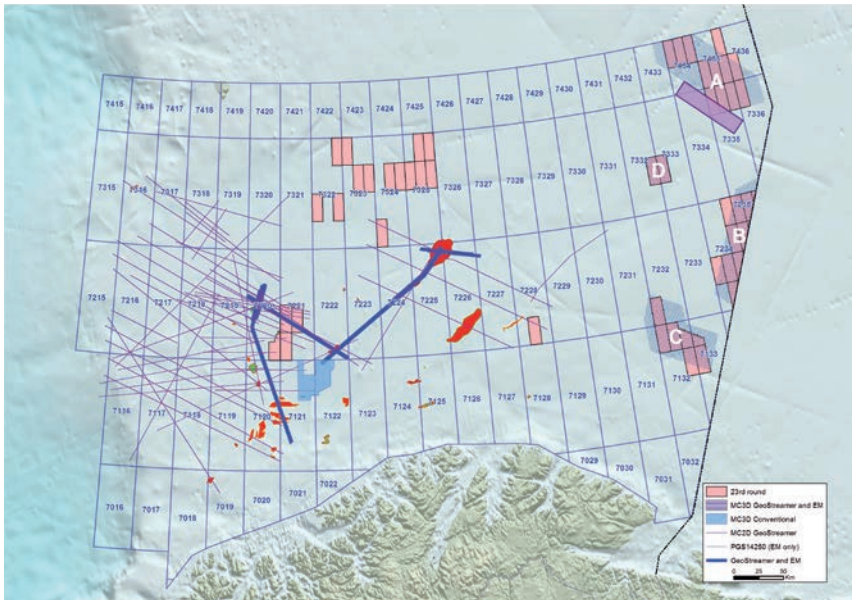

Figure 1 *Towed Streamer EM data in the Barents Sea in relation to blocks nominated for inclusion in the 23rd licensing round.*

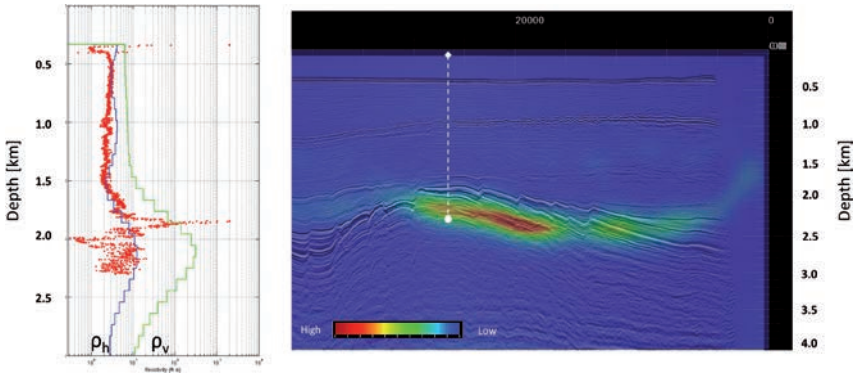

Figure 2 *An illustrative resistivity section determined using unconstrained inversion of Towed Streamer EM data acquired over the Snøhvit-Albatross structure in the Barents Sea. The colour bar highlights the highest resistivity values only – there are additional variations of resistivity that are not shown by this choice of display. The vertical axis is depth [m]; the horizontal axis is profile distance [m]. The seismic data in the background is full stack broadband dual sensor seismic.*

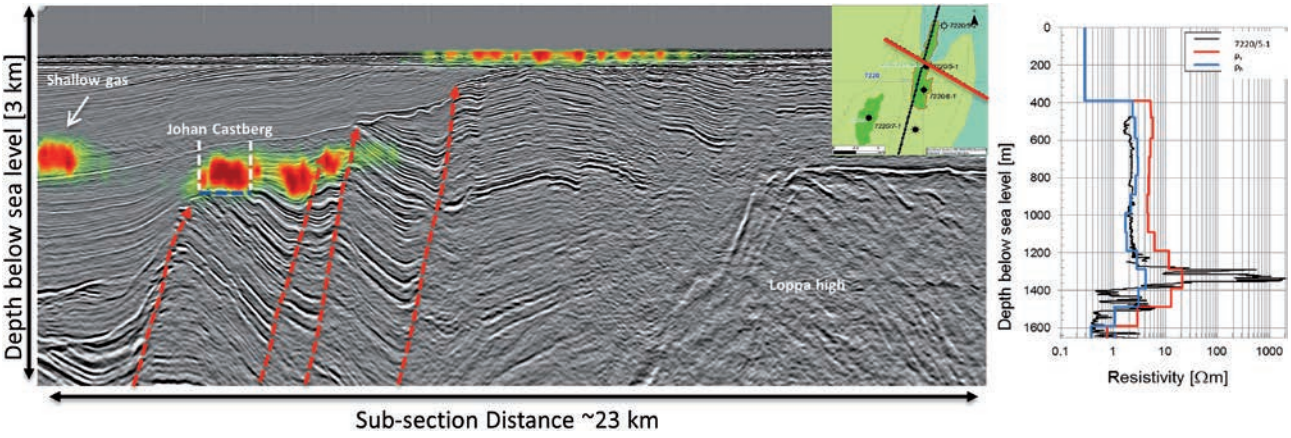

Figure 3 *Apparent anisotropy anomalies in the Johan Castberg area (left) and a comparison (right) between the logged and Towed Streamer EM anisotropic resistivity. Anisotropy less than 5 has been made transparent..*

For unconstrained 2.5D inversion we do not use a structured start model: the inversion is initiated from a half space. Convergence can be accelerated if an appropriate starting half-space resistivity is used (e.g., so that the amplitude levels of the measured and modelled data are similar at the start of the inversion). The only fixed resistivity model parameters are the water resistivity and water depth. The water depth is fixed on the basis of the measured echo-sounder data. The water resistivity is fixed on the basis of measured seawater resistivity-depth profiles taken daily by the survey guard vessel at different locations throughout the survey area. We find that a two-layer sea-water resistivity model is usually sufficient in shallow water.

To illustrate the kind of results we expect, we now consider two cases over known discoveries in the Barents Sea, and one from the frontier area of the Barents Sea South East.

Case 1: Snøhvit, Barents Sea

Snøhvit is a gas field with a thin underlying oil zone. It was discovered in 1984, and is located in the central part of the Hammerfest Basin in water depths of 310-340 m.

In Figure 2 we show the vertical resistivity section in the vicinity of the Albatross structure. There is an obvious deep resistivity anomaly that is robust, and structurally conformant. We did not traverse well locations directly, but the survey line passes quite close to two well locations. Consequently, shown in Figure 2 are the logged resistivity from the 7120/9-1 well, and the horizontal and vertical resistivity re-covered using unconstrained inversion. It is evident that the horizontal resistivity is very close to the logged resistivity depth trend. The vertical resistivity indicates a general background/over-burden anisotropy of about 2-3 (e.g. $\rho_v \sim= 2\rho_h$). At the reservoir level then there is an increase of both the horizontal and vertical resistivity, but the largest increase is in the vertical component of resistivity.

Case 2: Johan Castberg

The Johan Castberg area is located in PL532 in the Norwegian sector of the Barents Sea. The discovery of the Skrugard accumulation (which now together with the Havis discovery is called Johan Castberg) was a major milestone in the exploration of the Barents Sea.

In Figure 3 we show the resistivity anomalies in the form of apparent anisotropy (the ratio of the vertical to horizontal resistivity). The survey line shown crosses the short axis of Skrugard (about 2km wide) near to the surface location of the 7220/5-1 appraisal well completed in 2012, and is approximately perpendicular to the geological strike direction. The

anisotropy has been co-rendered with depth stretched (using the velocities from seismic processing) dual sensor seismic data.

The largest apparent anisotropy is restricted to the precise lateral location of Skrugard. At the appraisal well location the top Skrugard reservoir level is 1276 m below mean sea level; the Oil Water Contact is at 1395 m. The apparent anisotropy anomaly is between 1200 and 1500 m.

Out-with the vicinity of the Skrugard reservoir there are additional apparent anisotropy anomalies. The anisotropy anomaly to the west of Skrugard is most likely due to shallow gas: there is obvious seismic amplitude brightening, and the interval is known to be gas prone. East of the Skrugard reservoir, the anisotropy anomalies appear to follow the fault blocks: here there is the possibility of resistive source rock thickening eastwards as well as additional accumulations of hydrocarbons. The obvious faults are thought to provide a migration route for gas, and this could explain the near sea-bed anomalies.

Also shown in Figure 3 are the logged resistivity and the horizontal and vertical resistivity re-covered using unconstrained inversion. Similar to the Snøhvit case, the horizontal resistivity is very close to the logged resistivity depth trend. The vertical resistivity indicates a general background anisotropy of about 3 ($\rho_v \sim= 3\rho_h$) as well as an increase in vertical resistivity over the depth interval of the Skrugard reservoir. The vertical resistivity is consistent with the logged values published by Løseth et al. (2014).

Case Study 3: Barents Sea South East

The Norwegian Sector of the Barents Sea South East has only been recently opened up for petroleum exploration: interested operators were invited to nominate blocks for inclusion in the 23rd licensing round in 2013. The blocks that were nominated for inclusion are shown in Figure 1.

In addition to the 3D seismic data acquired as part of the 'group shoot' – a single acquisition project operated by Statoil on behalf of 33 companies – PGS acquired nearly 12,000 km^2 of 3D Towed Streamer EM data, with a line spacing of 1.25 km. These data are being inverted in 3D using the methodology outlined by Zhdanov et al. (2014). A key feature is the footprint methodology where the inversion of each area is performed all at once, but the modelling domain is decomposed into numerous sub-domains based on sensitivity measures. This enables large-scale inversion.

In Figure 4 we show an example depth slice through a 3D vertical resistivity model from the Barents Sea South East. There appear to be a combination of regional features, and localized zones of increased resistivity. The next step will be to integrate the resistivity models with the 3D seismic data to start a joint interpretation.

Implications for frontier exploration

The Snøhvit and Johan Castberg cases demonstrate that we can expect to gain useful insights into the prospectivity of an area if we can combine the sub-surface resistivity models with seismic data - for example, if we have good structural conformance of high resistivity in a rotated fault block or structural high, then the feature may be worthy of further investigation as a potential prospect.

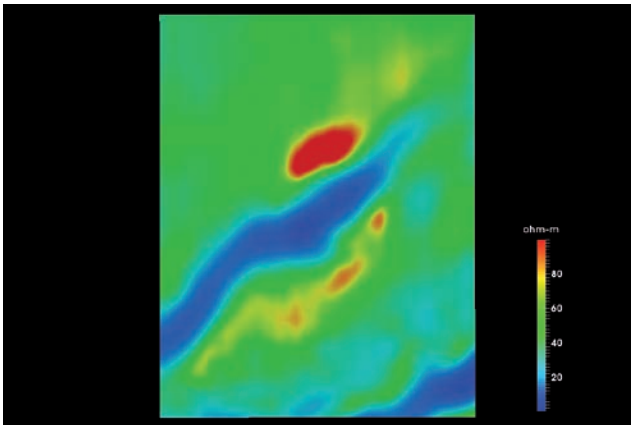

Figure 4 *An illustrative depth slice through a 3D resistivity volume determined using 3D inversion Towed Streamer EM data in the Barents Sea.*

Indeed, both the Snøhvit and Johan Castberg cases indicate that even in relatively complex geological settings then unconstrained inversion can produce sub-surface resistivity sections (and volumes) that are structurally conformant, well registered in depth, and consistent with the logged resistivity depth trend. In addition, the Johan Castberg case indicates that we are able to recover the sub-surface anisotropy. So, in the early exploration phase of a frontier area we should be able to use the sub-surface resistivity models with confidence.

Geological knowledge of the Barents Sea South-East is relatively limited, although there are analogue wells in both the Russian and Norwegian sectors. Now that there is a combination of 3D seismic and Towed Streamer EM data there is a unique opportunity to exploit the added information offered by resistivity models derived from Towed Streamer EM measurements early in the exploration workflow, where the ranking is at the block rather than prospect level. There is the potential to use the resistivity information, together with an interpretation of the seismic data to evaluate blocks e.g., by identifying blocks which possess a combination of acoustic and electromagnetic features of interest e.g., structural high combined with high resitivity, or an interval of low acoustic impedance and Vp/Vs ratio, but high resistivity.

Integration of Towed Streamer EM and dual-sensor seismic data

As we have shown, unconstrained inversion can certainly recover a useful, informative, smoothed image of sub-surface resistivity, but it may not resolve complex structures. It is relatively well known that the quantity constrained best by CSEM data is the transverse resistance (resistivity thickness product); resistive features can be smeared vertically (e.g.,

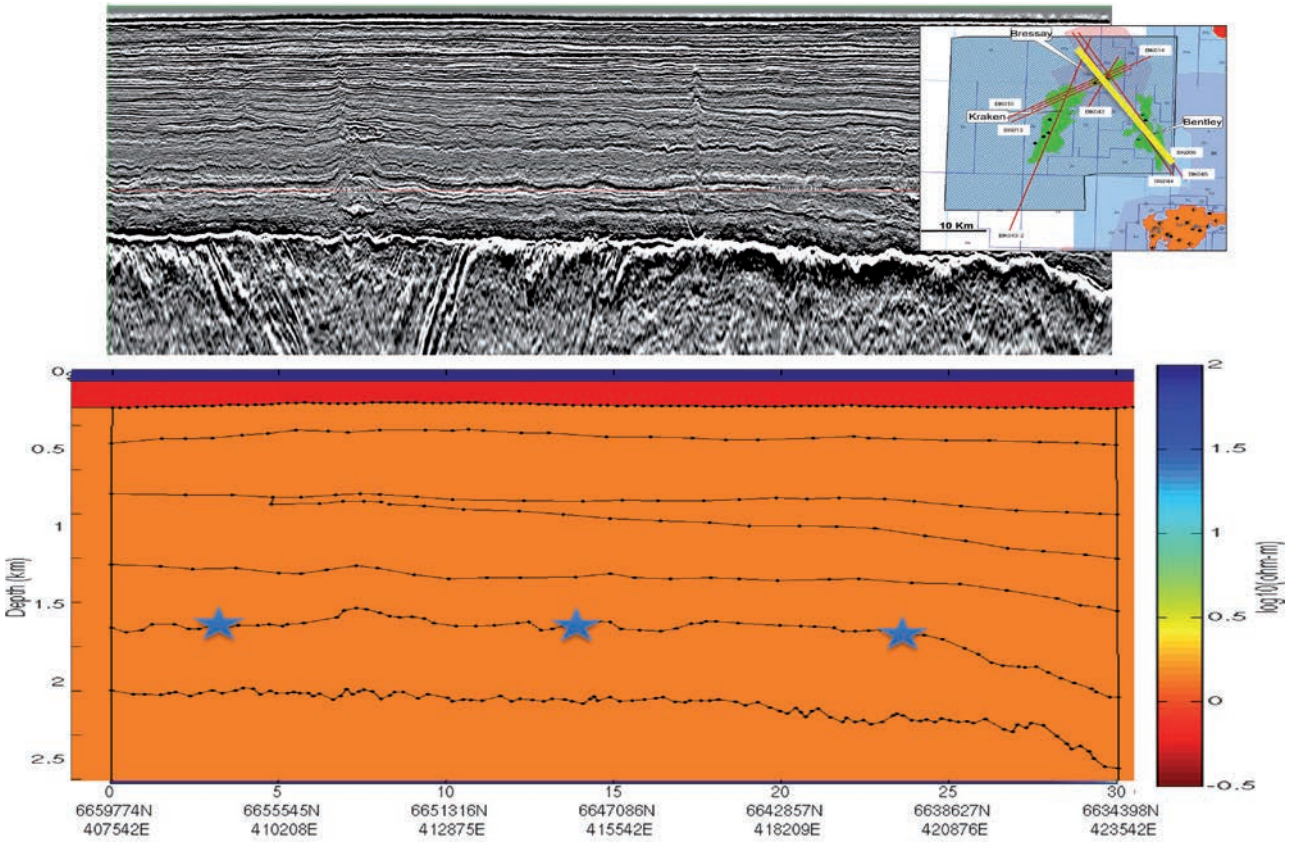

Figure 5 *An illustrative setup for conducting seismic guided inversion. The Top panel shows the coincident broadband dual-sensor seismic section in depth; the bottom panel shows the interpreted seismic horizons extracted from the top and adopted for guiding the inversion. The stars indicate the seismically defined top reservoir interface. Note that inversion starts from a 1 Ohm m half-space.*

MacGregor and Tomlinson, 2014, and references therein). The higher resolution of the seismic image makes it possible to suggest the most appropriate locations of potential resistivity contrasts. The integration of seismic and CSEM data enables the strengths of each data type to be fully exploited. Combining the two types of data should also improve fluid detection and provide different and complementary images of the geology.

While there are several methods for integration of EM and seismic data, and the choice of method depends on the task at hand, we have developed a workflow to make the inversion-based EM and seismic integration process more data and information-driven and less *a priori* model-driven. The seismic guided inversion (see Du and Hosseinzadeh, 2014) aims to facilitate an optimal procedure to combine the complementary information from dual-sensor seismic and the Towed Streamer EM data, with the seismic data best at constraining structure, and the EM data best at constraining resistivity. In summary, the inversions are guided by the seismic data to find the stratigraphic boundaries, whereas the resistivity variations within the overburden layers are guided by plausible lower and upper bounds on resistivity suggested by proceeding unconstrained inversions.

Outline of workflow

There are four main elements of the seismically guided inversion workflow (see also Figure 5):

1. Unconstrained Inversion: as we have demonstrated at the very least we can recover information about the resistivity depth trend and spatial variation of resistivity using unconstrained inversion. The unconstrained inversion can therefore provide upper and lower bounds on the sub-surface resistivity (i.e., parameter constraints) over a given depth interval.
2. Main seismic horizons in depth: these serve the purpose of parameterizing the resistivity model based on structure as well as providing possible electromagnetic boundary surfaces that divide different stratigraphic intervals so that the parameter constraints from the unconstrained inversion can be applied over the appropriate depth intervals.
3. Seismic guided inversion: is initiated by adopting a sparse-layer depth model defined by a high-resolution seismic image, as described in Step 2, to suggest resistivity boundaries for the EM inversion. Whereas a conventional constrained inversion adopts this model to prejudice the EM inversion's roughness penalty to force resistivity variations to follow the major acoustic

boundaries, in our workflow the resistivity variations within these layers are accommodated by the lower and upper boundaries suggested by the unconstrained inversion (Step 1), while the remaining regions are all set as free parameters for inversion.

4. Joint interpretation of the Seismic and EM data: as we have seen we can achieve good structural conformance between the sub-surface resistivity and seismic boundaries even when using unconstrained inversion. However, as complexity increases we must recognise that the smoothness of an unconstrained inversion may not be an ideal representation of the sub-surface resistivity. So, we may need to interpret both the seismic and EM data together, for example, by matching stratigraphic levels.

We now illustrate the practical implementation of the seismically guided inversion workflow.

A North Sea case study: Bressay, Bentley and Kraken area

Bressay, Bentley and Kraken (BBK) are three Heavy Oil (11-12 API; viscosity of 1000 centipoise) reservoirs located on the western edge of the Viking Graben in UK Quadrant 9 of the North Sea; see Figure 6. The reservoirs straddle a depth range of about 1000-1300 m, beneath a shallow water column of depth 90-130 m. The Heimdal Formation, Late Palaeocene, BBK heavy oil sands are difficult to image with seismic data alone due to the low acoustic impedance (AI) contrast with the surrounding shale; see for example Du and Hosseinzadeh (2014).

In Figure 7 (upper panel) the unconstrained inversion of one Towed Streamer EM survey profile traversing Bressay and Bentley has faithfully recovered the resistive basement since it has the largest impact on the data responses. It has also revealed two resistive anomalies with significantly increased vertical resistivity in the overburden. While these resistive anomalies are located at the lateral position of Bressay and Bentley reservoirs, their depths are inconsistent with the known reservoirs.

In the guided inversion the boundaries between the interbedded sands and shales in the overburden of Bressay and Bentley were defined by the post-stack dual-sensor seismic data, and the anisotropic resistivity variations within the layers above the top reservoir horizon (indicated by the stars in Figure 5) were guided by the lower and upper bounds placed on the resistivity (Item 2 in the outline workflow) as determined from the unconstrained inversion (Item 1 in the outline workflow). The remaining regions are all set as free parameters (i.e., the space below the stars in Figure 5). Note the seismic boundaries adopted here are free (not fixed) parameters, and have been adopted only for the purpose of 'guiding' the EM inversion that the geological interfaces mapped by seismic data may also be potential EM boundaries.

In the lower panel of Figure 7, the final result of the seismically guided inversion is shown. The inversion recovers the reservoirs by showing the prominent high resistive anomalies coinciding perfectly with the position of the main reservoir structures as shown by the seismic data. Compared to unconstrained inversion, the boundary between the overburden and the underlying formation constrained by the seismically guided inversion is much more consistent with the seismic image.

The inversion workflow is data driven, and it offers the potential to improve the resolution of the sub-surface

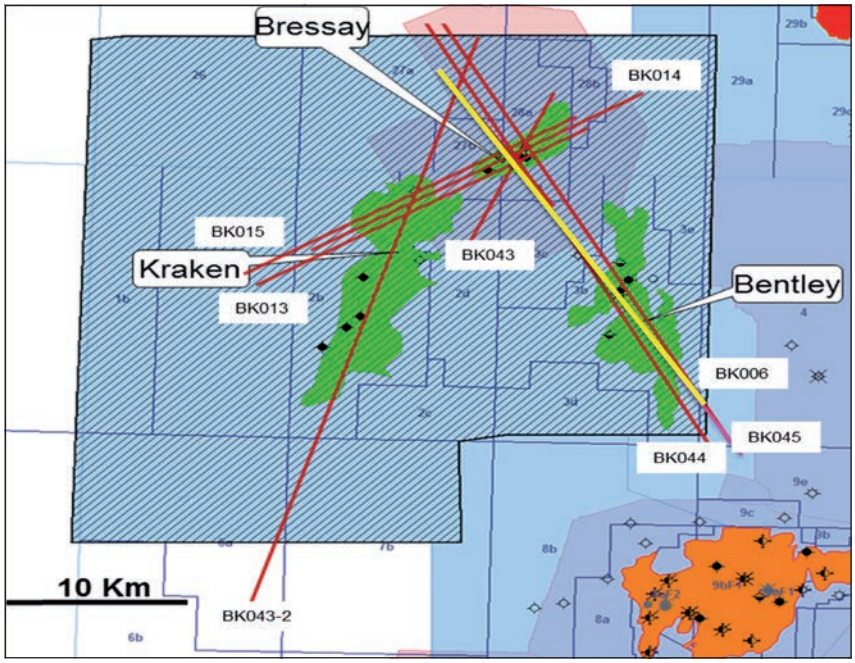

Figure 6 *Map of the Bressay, Bentley and Kraken area. The red lines show Towed Streamer EM survey lines; the yellow line is the focus of the case study.*

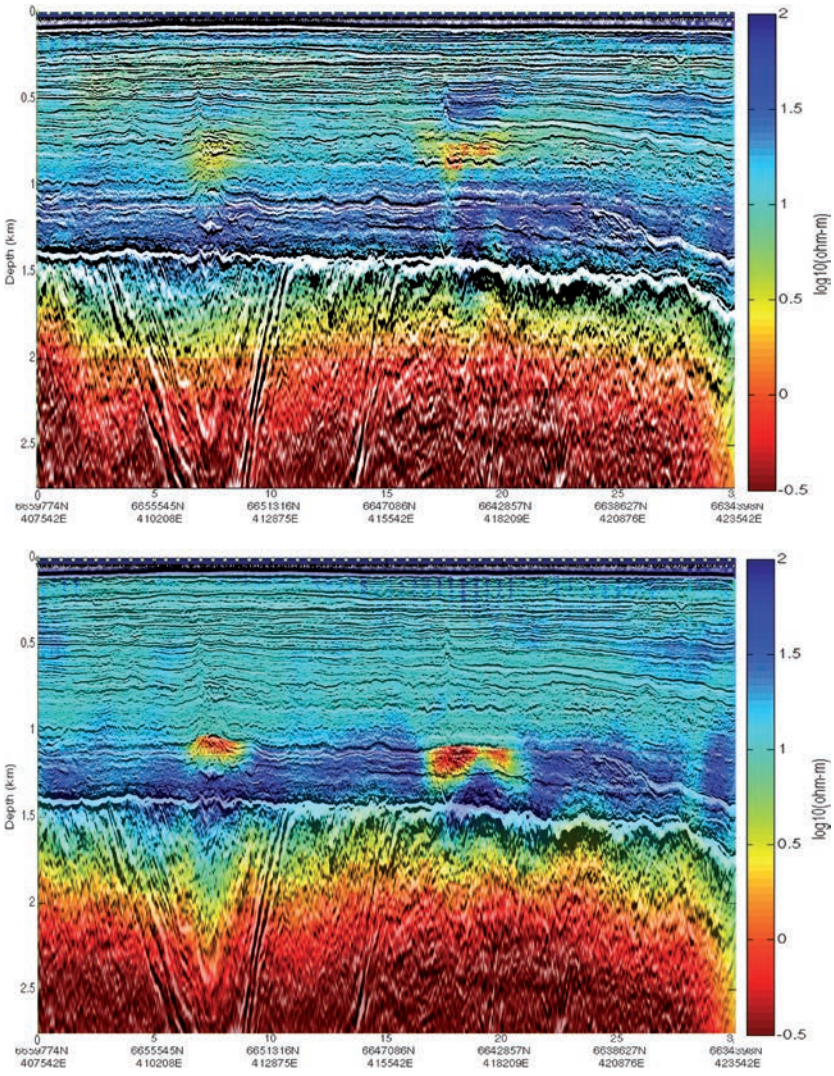

Figure 7 *Vertical resistivity overlain on co-incident depth converted full-stack broadband dual sensor data determined using unconstrained (upper panel) and seismically guided (lower panel) inversion for a survey line traversing the Bressay-Bentley reservoirs.*

resistivity model. In addition, we believe that it also could be applied in a frontier exploration setting given both seismic and EM data. No information from well logs is required (although of course well logs could be used to e.g., ensure that horizons are registered in depth as accurately as possible).

On the benefits of high data density

As we have seen, Towed Streamer EM resistivity models contain valuable information about the sub-surface resistivity. One of the benefits of Towed Streamer EM acquisition is the exceptionally dense spatial data sampling (with a shot spacing of 250 m, and up to 72 electric field channels). In this section, we illustrate how the dense in-line spatial sampling translates into value for the end user with resistivity models that have improved resolution and precision in comparison to those derived from a coarser data sampling. In addition, to underpin the practical case study examples, we show how the anisotropy of the sub-surface is constrained by Towed Streamer EM data by examining the resolution of the vertical and horizontal resistivity as a function of depth and position along a real survey line.

The effect of in-line spatial data density

First, we examine how the sub-surface model of resistivity is degraded as the in-line shot spacing is increased from 250 m to 1000 m. We use an unconstrained inversion of Towed streamer EM data from one of the survey lines over the Alvheim Boa field, located within the Norwegian sector of the North Sea; see Figure 8.

The Alvheim reservoir is of sandstone type with a burial depth of 2100 m below the mud-line. The reservoir reaches its maximum thickness (red in Figure 8) immediately to the west of the survey lines. The water depth along the survey profile varies between 110 and 125 m. The overburden consists of shale and sandstone layers. See Mattsson et al. 2013, for more details.

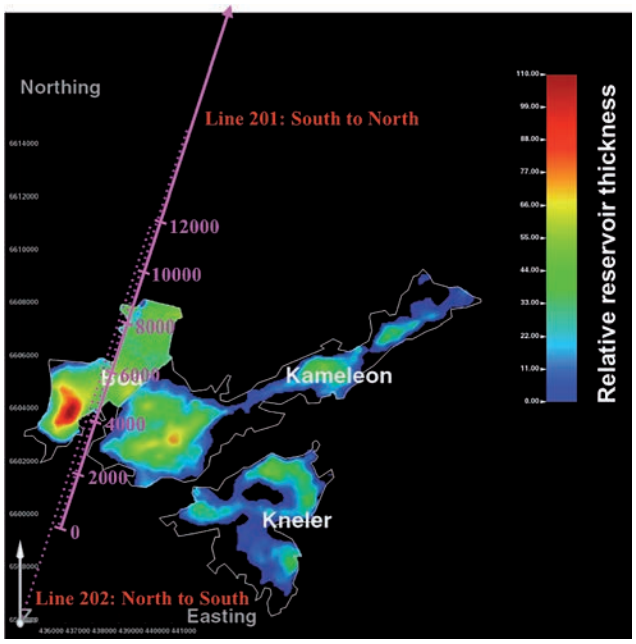

Figure 8 *A thickness map of the Alvheim Boa reservoir including two towed streamer EM survey lines.*

The Towed Streamer EM data consist of frequency responses from 60 source-receiver gathers (so called 'shots') spaced every 250 m in the in-line direction. Each source-receiver gather consists of frequency responses from nine offsets between 1450 m and 7500 m, and five frequencies from 0.15 Hz to 0.75 Hz. The Towed Streamer EM data were inverted following the unconstrained workflow outlined previously.

We examine two cases to illustrate the benefits of data density. First, we invert the dense data case with a 250 m in-line shot spacing; the depth sections of horizontal and vertical resistivity as a result of the inversion are shown in Figure 9. We then decimate the data and only use every fourth shot in the inversion i.e. the in-line shot separation is increased from 250 m to 1000 m, while retaining the same offsets and frequencies as before. The inversion results for the decimated case are shown in Figure 10.

First, let us examine the resistivity sections for the dense case. The vertical resistivity (upper panel; Figure 9) shows a resistive anomaly of 5-6 Ohm m at a depth of 2 km below the mud-line that coincides laterally with the Boa reservoir location. There is also a layer of slightly higher resistivity at 1000 m depth corresponding to a sand layer in the overburden. The horizontal resistivity (lower panel; Figure 9) is somewhat lower throughout the cross section.

If we now compare the decimated and dense cases we can see that in the decimated case the overburden is irregular, patchy and does not look geologically consistent. For example, there are obvious near-surface anomalies that are not present at all in the dense case. In addition, while there is still a vertical resistivity anomaly coinciding with the Boa reservoir it is less pronounced (upper panel; Figure 10). This brief comparison highlights the importance of dense spatial sampling. In particular, we conclude that a 1000 m shot separation is too sparse.

Resolution and precision of resistivity models

The quality of the inversion results for the two cases is quantified by calculating the resolution matrices corresponding to the resistivity models from inversion. The starting point is the model update equation in the inversion algorithm. In this case it read like:

$$m_{k+1} = S_k^{\otimes} W(d - F(m_k) + J_k m_k) \quad (1)$$

where

$S_k^{\otimes} = \left[\mu(\partial^T \partial) + S_k{}^T S_k\right]^{-1} S_k{}^T$ = regularized inverse
$\mu(\partial^T \partial)$ = smoothing regularization
$S_k = WJ_k$

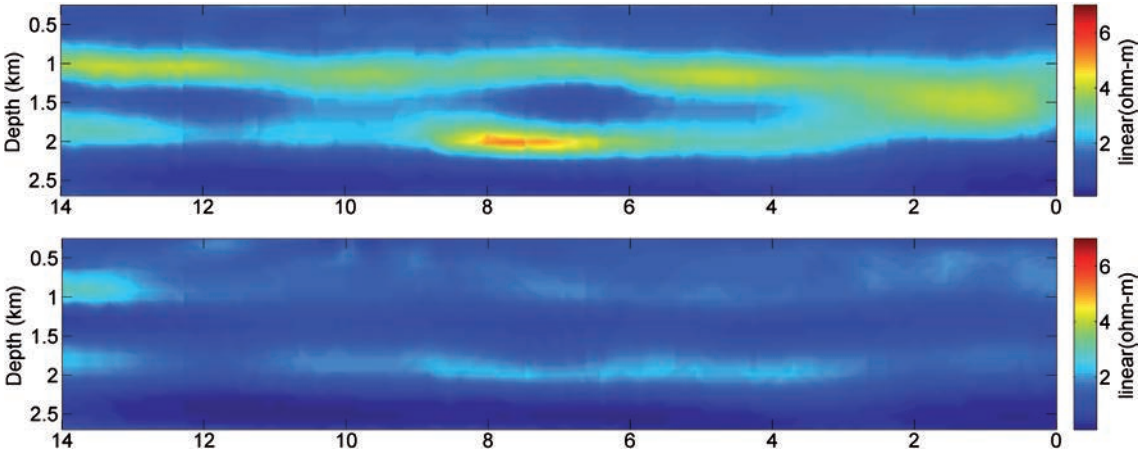

Figure 9 *the vertical and horizontal inversion results with a shot separation of 250 m. The horizontal axes show the distance in km from north (right) to south (left).*

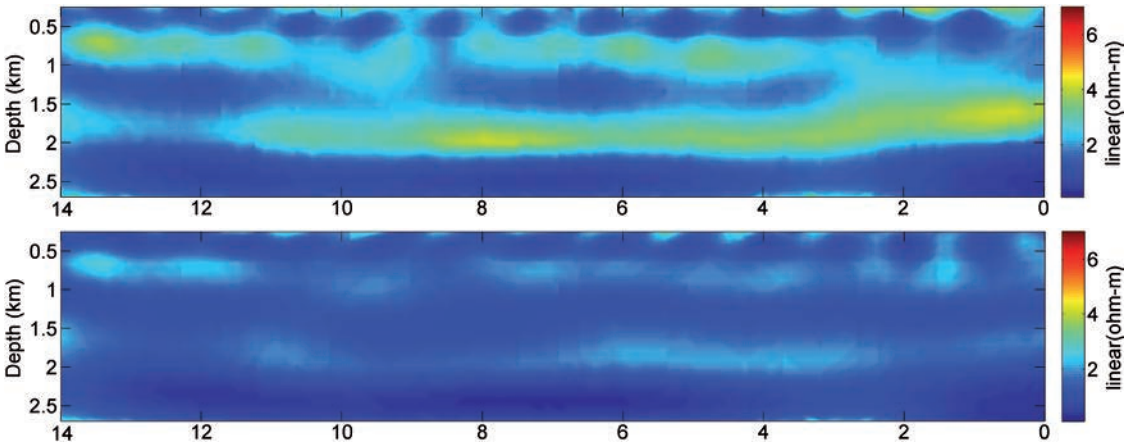

Figure 10 *the vertical and horizontal inversion results with a shot separation of 1000 m. The horizontal axes show the distance in km from north (right) to south (left).*

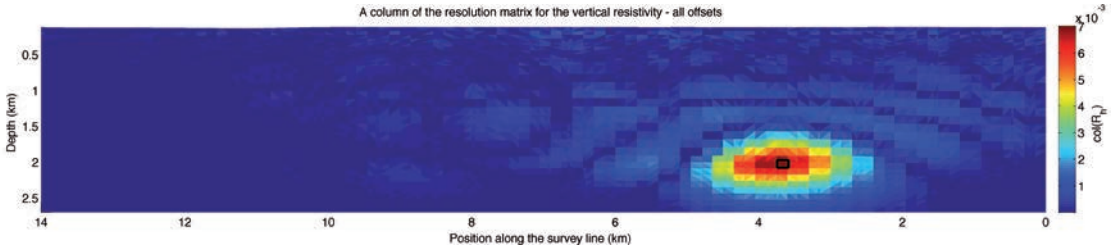

Figure 11 *the resolution spread of the value in the cell with a black rectangle.*

J_k = Jacobian matrix = $J_{ij} = \dfrac{\partial F_i(m_k)}{\partial \log_{10} \rho_j}$

W = Weight matrix = diag$(\dfrac{1}{\sigma_i})$

$F(m_k)$ = Modelled frequency response

d = Frequency response from measured data

σ_i = Standard deviation of d_i

ρ_j = Resistivity

m_k = Model vector $k = (\log_{10} \rho_j)_k$

The model after the final iteration of (1) is now assumed to be close to an exact model of the problem satisfying the data. The following relation can then be derived:

$$m_{k+1} = R_k m_{exact} + S_k^{\otimes} W n \qquad (2)$$

where

$$R_k = S_k^{\otimes} S_k$$

n = the uncertainty in the frequency responses (3)

The matrix R_k is the resolution matrix of the inversion, (Hansen, 1998). It reveals how well the inversion algorithm can recover a resistivity model. In fact the resolution matrix quantifies the smoothing regularization effect in this case. This means that R_k maps the spreading of resistivity elements in m_{exact} to the model vector m_{k+1}. The resolution is perfect if the resolution matrix equals the unit matrix. The inversion has then recovered the exact resistivity model perfectly. Hence, the main diagonal of R_k quantifies how well each cell in the inversion grid is resolved. A number less than one in a cell means that the resistivity value of the exact model is spread out over a number of adjacent cells in the inversion result. Each column in the resolution matrix shows how the value in a cell in the exact model is spread to several cells in the inversion model. This is exemplified in Figure 11 where it can be seen that the value in the cell with the black rectangle is less than one and is spread out to the adjacent cells. This is a direct effect of the smoothing regularization of the inversion. It also means that the resolution is smeared out over the cells with non-zero values from the optimal resolution of one cell.

The resolution of the resistivity values in each cell (i.e., the diagonal of the corresponding resolution matrices) of the dense and decimated cases (Figure 9 and Figure 10 respectively) is shown in Figure 12 and Figure 13 respectively. It can be seen that the resolution is close to one in the first 200-300 m of the overburden. The resolution then decreases towards 0.001 below 2200 m for the vertical resistivity with 250 m shot spacing. This means that a vertical resistivity value in a cell below 2200 m in an exact model is spread out over numerous cells. The spread implies that only large-scale structures of constant vertical resistivity can be resolved below this depth. Hence, the precision is degraded below 2200 m in this case for the vertical resistivity. The resolution for the horizontal resistivity is better

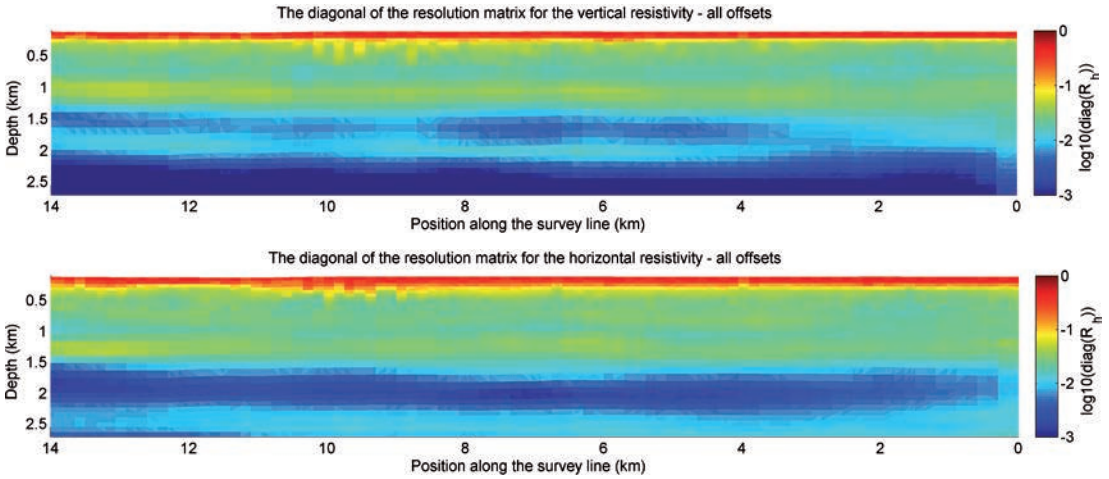

Figure 12 *The resolution of the vertical and horizontal resistivity values with 250 m shot spacing. The colour scale denotes log_{10} log_{10} values.*

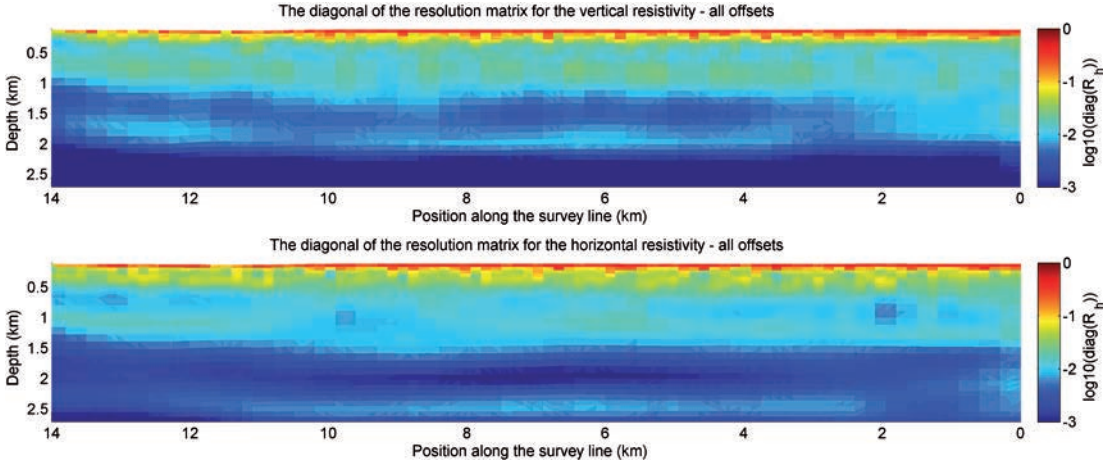

Figure 13 *the resolution of the vertical and horizontal resistivity values with 1000 m shot spacing. The colour scale denotes log_{10} log_{10} values.*

at this depth and is similar to the vertical resistivity resolution in the overburden. That the resolution of the vertical and horizontal resistivity in the over and under-burden is similar indicates that the sensitivity to the horizontal resistivity is nearly the same as for the vertical resistivity. The sensitivity to a change in horizontal resistivity appears to decrease relative to the vertical resistivity only in the resistive sand layer at 1000 m, and at the resistive anomaly corresponding to the Boa reservoir which is to be expected as CSEM methods are less sensitive to the horizontal resistivity of a thin horizontal structure than the vertical resistivity of the same structure.

The resolution decreases by a factor of 5-10 in the whole subsurface for both the vertical and horizontal resistivities when the shot separation is increased to 1000 m; Figure 13. This means that the sensitivity decreases and as a consequence the inversion results are degraded as is indicated by the results presented in Figure 10. Hence, the spatial data density available with the towed streamer EM acquisition system increased the resolution and accuracy of the inversion results by a factor of 5-10 in this case.

Summary and conclusions

The sub-surface resistivity determined by unconstrained inversion of Towed Streamer EM data is consistent with the resistivity measured in the well, the regional geological background as well as known accumulations of hydrocarbons. We can demonstrate by example that we can re-cover resistivity anisotropy that is consistent with log, and that the underlying sensitivity to the vertical and horizontal resistivity is similar.

The resistivity sections may be further enhanced when only weak structural constraints are employed. Thus, valuable and independent information can be gained in a timely fashion form unconstrained inversion with the possibility that more value can be extracted from a combination of seismic and Towed Streamer EM data e.g., mature leads into prospects.

One of the benefits of Towed Streamer EM acquisition is the exceptionally dense spatial data sampling: we have shown how the data density improves the resolution and precision of the sub-surface resistivity models in comparison to those derived from a coarser data sampling.

Acknowledgments

We would like to thank Petroleum Geo-Services for permission to publish this work, and to our colleagues Anwar Bhuiyan, Eivind Vesterås and Jenny-Ann Malmberg who provided the Barents Sea case study examples. TechnoImaging, LLC performed the 3D inversion presented in the Barents Sea South East case study: we would also like to thank Masashi Endo and David Sunwall in particular for their hard work and contribution to the project. The MARE2DEM Finite Element modelling and inversion code was developed by the Scripps Seafloor Electromagnetic Methods Consortium, and we thank our fellow consortium members and Scripps for developing MARE2DEM on behalf of the whole CSEM community.

References

Du, Z. and Hosseinzadeh, S. [2014] Seismic guided EM inversion in complex geology: Application to the Bressay and Bentley heavy oil discoveries, North Sea. *76th EAGE Annual Conference & Exhibition*, Extended Abstracts.

Hansen P.C. [1998] *Rank-Deficient and Discrete Ill-Posed Problems*. ISBN 0-89871-403-6, SIAM.

Key K., Du Z., Mattsson J., McKay, A. and Midgley, J. [2014] Anisotropic 2.5D inversion of Towed Streamer EM data from three North Sea fields using parallel adaptive finite elements. *76th EAGE Annual Conference & Exhibition*, Extended Abstracts.

Løseth, L.O., Wiik, T., Olsen, P.A and Hansen, J.O. [2014] Detecting Skrugard by CSEM – Prewell prediction and postwell evaluation. *Interpretation*, **2** (3), SH67–SH78.

MacGregor, L. and Tomlinson, J. [2014] Marine controlled-source electromagnetic methods in the hydrocarbon industry: A tutorial on method and practice. *Interpretation*, **2** (3), SH13–SH32.

Mattsson, J., Englemark, F. and Anderson, C. [2013] Towed streamer EM: The challenges of sensitivity and anisotropy. *First Break*, **31**, 155–159.

McKay, A, Bergh, K.F. and Bhuiyan, A.H. [2014] Determining resistivity from Towed Streamer EM data using unconstrained inversion – Tie to well and discovery examples. *76th EAGE Annual Conference & Exhibition*, Extended Abstracts.

Ramananjaona, C., MacGregor, L. and Andreis, D. [2011] Inversion of marine electromagnetic data in a uniaxial anisotropic stratified earth. *Geophysical Prospecting*, **59**, 341–360, doi: 10.1111/j.1365-2478.2010.00919.x.

Zhdanov, M.S., Endo, M., Yoon, D., Cuma, M., Mattsson, J. and Midgley, J. [2014] Anisotroic 3D inversion of towed streamer electromagnetic data: Case study from the Troll West Oil Province. *Interpreta*tion, 2 (3), SH01–SH17.